Supporting Information

Narikawa et al. 10.1073/pnas.1212098110

SI Results and Discussion

The green/red-type CBCRs represented by CcaS and RcaE do not retain the highly conserved Asp residue (Asp291 in AnPixJg2 and Asp492 in TePixJg) (1, 2). Instead, they have a highly conserved glutamic acid residue adjacent to the Asp. Furthermore, the highly conserved His residue (His322 in AnPixJg2, His523 in TePixJg) that stabilize the A-B-C ring plane is instead Leu in such green/red-type CBCRs. Hence, the chromophore structure and protonation state of the rings may be differently arranged in these CBCRs and may be the reason why the 15Z form is significantly blue-shifted in comparison with the Pr form of phytochromes.

The insert Cys-type CBCRs are also thought to form transient or stable attachments in the blue-shifted forms (3). In this case, the use of a different, independently evolved second Cys residue may be the reason why the chromophore is PCB not PVB. The insertion position of the insert Cys-type CBCRs corresponds well to the short insertion region in the third β strand of AnPixJg2 (3). Based on this alignment, the insert Cys residue is too far from the C10 of PCB to form an intramolecular covalent bond as in TePixJg. Thus, intermolecular covalent bonds in a dimer unit may occur in the case of the insert Cys-type CBCRs. Alternately, the large insertion loop in such proteins may wrap around the GAF fold to allow the insert-Cys thiol access from the other side, exploiting the solvent accessibility of the A ring in CBCRs relative to phytochromes.

Spectral and biochemical analyses of diverse CBCRs are ongoing, and many proposed photosensory mechanisms have been presented. The structural information presented in this study will be very helpful for this work. It should now be possible to identify the core chromophore-binding pocket in all linear tetrapyrrole-based photoreceptors using computational approaches. These analyses, together with site-directed mutagenesis and biochemical and spectroscopic studies, will shed light on the general and diverse aspects of the linear tetrapyrrole-based photoreceptors, leading to a deeper understanding of the photosensory mechanism.

SI Materials and Methods

Protein Preparation and Crystallization. Purification and crystallization of His-tagged AnPixJg2 were previously described (4). His-tagged TePixJg was first purified by Ni-affinity column from *Synechocystis* sp. PCC 6803 as previously reported (5), followed by further purification by using a Superdex 75 gel filtration column (GE Healthcare) with removal of imidazole and glycerol. The final buffer was composed of 20 mM Hepes (pH 7.5) and 100 mM NaCl. These purified proteins were finally concentrated up to 10 mg mL^{-1}. The crystallization was carried out at 4 °C under the dark or the safety light (red light for TePixJg Pg) by the hanging drop vapor diffusion method. Crystallization droplets were prepared on siliconized coverslips by mixing 1 μL of protein solution with 1 μL of reservoir solution and were equilibrated against 180 μL of the same reservoir solution. Large pink crystals of TePixJg Pg were prepared with 100 mM Mes buffer (pH 5.8) containing 1.15 M ammonium sulfate as precipitant.

For cryo-protection, the crystals of AnPixJg2 and TePixJg were soaked for a few minutes in each reservoir solution containing 20% (vol/vol) glycerol. The crystals were mounted in a nylon loop and then flash-frozen in liquid nitrogen.

Structure Determination. Two sets of X-ray diffraction data from a crystal of AnPixJg2 were collected at 100 K on the beamline BL5A of the Photon Factory for the SAD-phasing as described previously (38). The structure of AnPixJg2 was determined by the single-wavelength anomalous diffraction (SAD) method using the bound iodide ion, because the crystals were obtained from an iodide-containing solution (Table S1). The determination of heavy-atom binding sites and the initial phase calculations were performed using SOLVE, and the density modifications and the initial model building were carried out using RESOLVE at a resolution of 1.8 Å (6). The overall figure of merit obtained with SOLVE and RESOLVE were 0.276 and 0.635, respectively. The ARP/wARP program was used for further model building (7). Iterative manual model building was carried out using the program COOT (8). The model was refined against the 1.8-Å native data set with the program Refmac5 (9). A randomly sampled 5% of the data were excluded throughout refinement and used to monitor the course of refinement. The final model included a single polypeptide chain [Ser (two amino acids after the 6His) – Thr388], one PCB molecule covalently linked to Cys321, one iodide ion and 175 water molecules, with an *R*-factor of 0.197 and a free-*R* factor of 0.224.

For TePixJg, X-ray diffraction data were collected at 100 K on the beamline BL17A of Photon Factory equipped with an ADSC Quantum 270 CCD detector and a Rigaku GN2 cryosystem. X-ray diffraction images were recorded with an oscillation angle of 1° and processed using the HKL2000 program package (Table S1). The crystal structure of TePixJg was determined by the molecular replacement method with a program Molrep in CCP4 (10), using the atomic model of the TePixJg apoprotein without the chromophore as the search model. The two polypeptide chains, related by a noncrystallographic twofold, existed in the crystallographic asymmetric unit. This crystallographic dimer was cross-linked through a disulfide bond of Cys-494, unexpectedly formed during crystallization. Early in the refinement with CNS program (11), a bound PVB was clearly seen and the chromophore was fitted manually to the density of each molecule. The iterative crystallographic refinement was performed against the 1.95 Å data set, using the programs of Refmac5 in CCP4 package and COOT (8, 10). Finally, TLS refinements were carried out using Refmac5 after adding solvent molecules. In the final electron density map, 136 water molecules and four sulfate ions were assigned in the asymmetric unit. R-factor of the final model is 0.190 (R_{free} = 0.229).

Statistics calculated with the program PROCHECK (12) showed that the model quality was beyond the normal standard in each case of AnPixJg2 and TePixJg. Protein-chromophore interactions were analyzed using HBPLUS with LigPlot^{+}. The structures are visualized, superimposed and measured using the software PyMOL to prepare the figures (http://pymol.org). The rmsd values are calculated by CCP4 program.

1. Hirose Y, Narikawa R, Katayama M, Ikeuchi M (2010) Cyanobacteriochrome CcaS regulates phycoerythrin accumulation in *Nostoc punctiforme*, a group II chromatic adapter. *Proc Natl Acad Sci USA* 107(19):8854–8859.
2. Hirose Y, Shimada T, Narikawa R, Katayama M, Ikeuchi M (2008) Cyanobacteriochrome CcaS is the green light receptor that induces the expression of phycobilisome linker protein. *Proc Natl Acad Sci USA* 105(28):9528–9533.
3. Rockwell NC, Martin SS, Feoktistova K, Lagarias JC (2011) Diverse two-cysteine photocycles in phytochromes and cyanobacteriochromes. *Proc Natl Acad Sci USA* 108(29):11854–11859.
4. Narikawa R, Muraki N, Shiba T, Ikeuchi M, Kurisu G (2009) Crystallization and preliminary X-ray studies of the chromophore-binding domain of cyanobacteriochrome AnPixJ from *Anabaena* sp. PCC 7120. *Acta Crystallogr Sect F Struct Biol Cryst Commun* 65(Pt 2): 159–162.

5. Ishizuka T, et al. (2006) Characterization of cyanobacteriochrome TePixJ from a thermophilic cyanobacterium *Thermosynechococcus elongatus* strain BP-1. *Plant Cell Physiol* 47(9):1251–1261.
6. Terwilliger TC (2003) SOLVE and RESOLVE: automated structure solution and density modification. *Methods Enzymol* 374:22–37.
7. Langer G, Cohen SX, Lamzin VS, Perrakis A (2008) Automated macromolecular model building for X-ray crystallography using ARP/wARP version 7. *Nat Protoc* 3(7):1171–1179.
8. Emsley P, Lohkamp B, Scott WG, Cowtan K (2010) Features and development of Coot. *Acta Crystallogr D Biol Crystallogr* 66(Pt 4):486–501.
9. Murshudov GN, et al. (2011) REFMAC5 for the refinement of macromolecular crystal structures. *Acta Crystallogr D Biol Crystallogr* 67(Pt 4):355–367.
10. Potterton E, Briggs P, Turkenburg M, Dodson E (2003) A graphical user interface to the CCP4 program suite. *Acta Crystallogr D Biol Crystallogr* 59(Pt 7):1131–1137.
11. Brunger AT (2007) Version 1.2 of the Crystallography and NMR system. *Nat Protoc* 2(11):2728–2733.
12. Laskowski RA, Moss DS, Thornton JM (1993) Main-chain bond lengths and bond angles in protein structures. *J Mol Biol* 231(4):1049–1067.

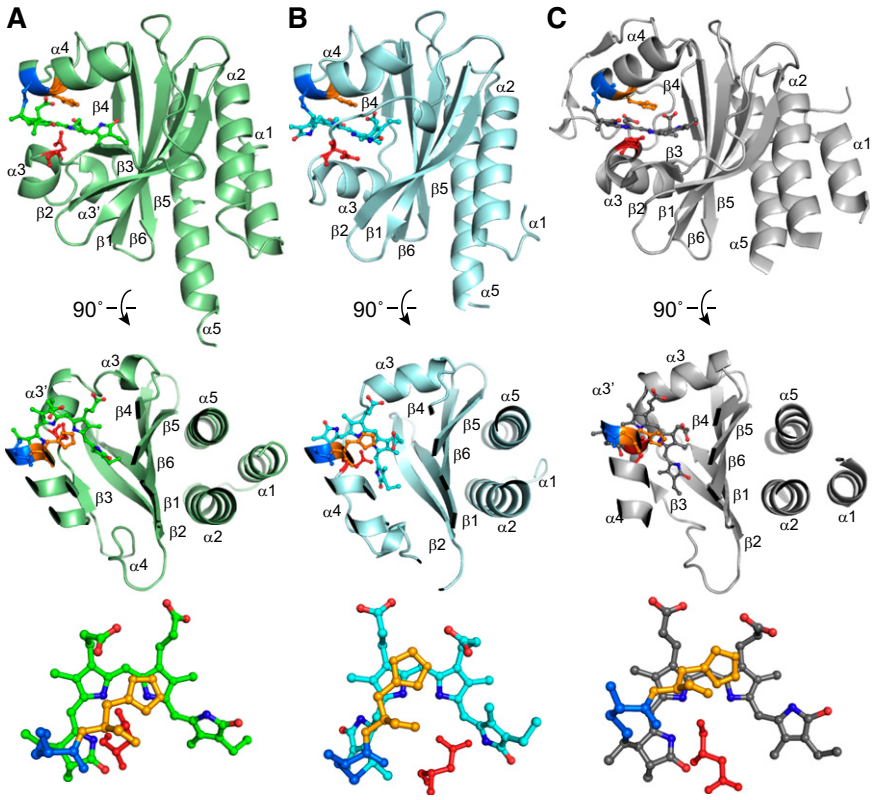

Fig. S1. Overall structures of the GAF domains of AnPixJg2 (*A*, green), TePixJg (*B*, sky blue), and Cph1g (*C*, gray) in Pr, Pg, and Pr forms, respectively. (*Top*) Side views of the overall structures. (*Middle*) Top views of the overall structures. (*Bottom*) Chromophores with key residues of Cys (blue), His (yellow), and Asp (red).

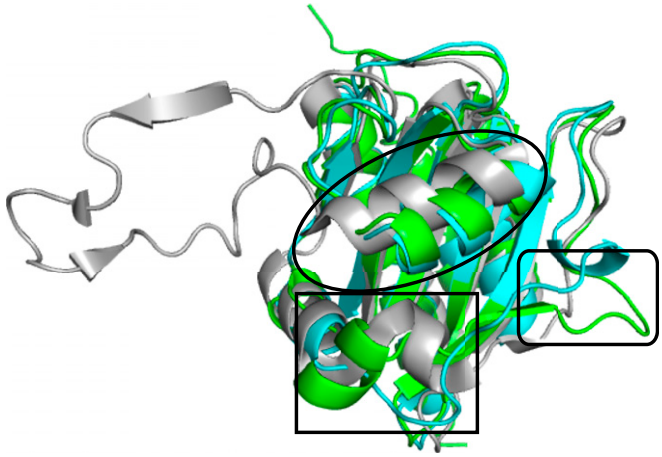

Fig. S2. GAF domains of AnPixJg2 (green), TePixJg (cyan), and Cph1g (gray) superimposed by overall structure. Open circle highlights the α4 region that is structurally altered between the phytochromes and CBCRs. Open square highlights the α3′ region that is diversified among the phytochromes and CBCRs. Open square with round edges highlights the β3 and short insertion regions.

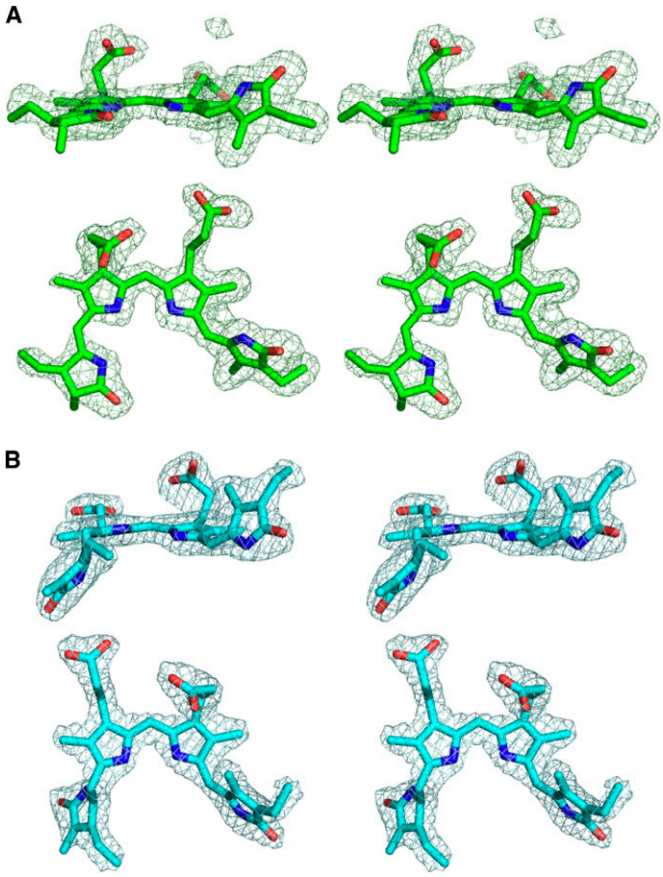

Fig. S3. AnPixJg2 PCB (*A*) and TePixJg PVB (*B*) with omit maps.

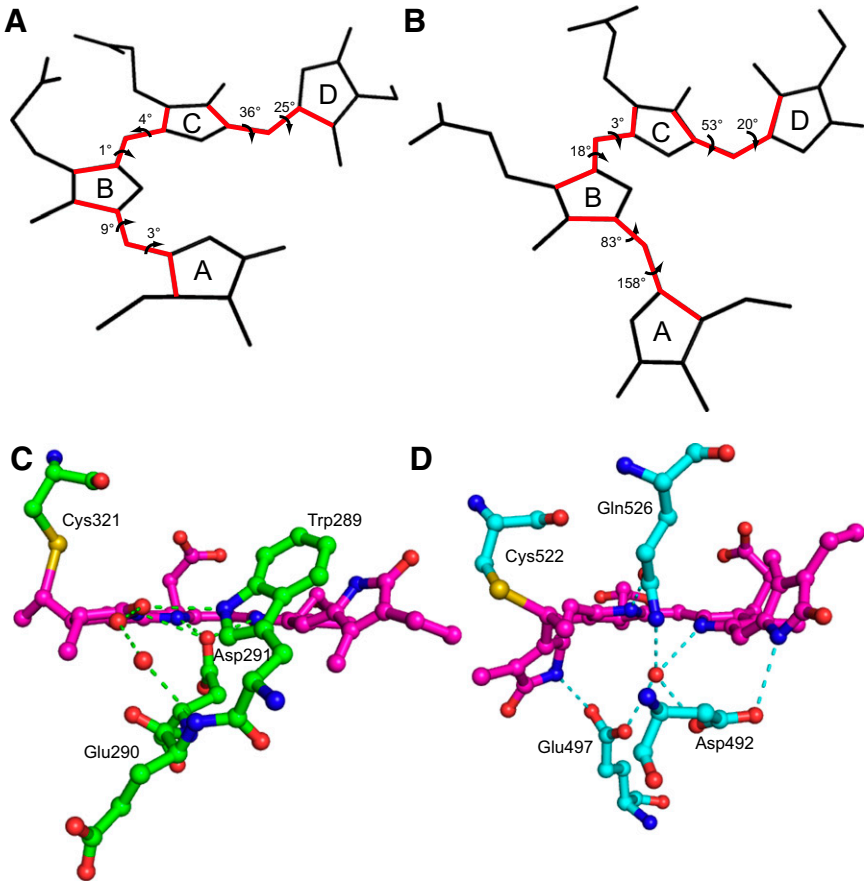

Fig. S4. Ring structures with dihedral angles (*A*, AnPixJg2 PCB; *B*, TePixJg PVB) and side view of chromophore-binding pockets (*C*, AnPixJg2; *D*, TePixJg).

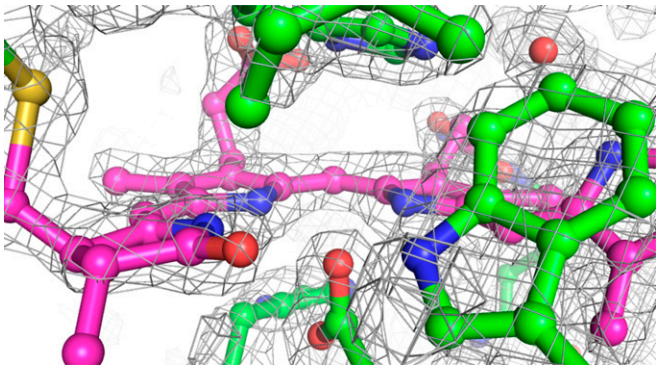

Fig. S5. PCB and surrounding residues of AnPixJg2 with electron density map that clearly show no pyrrole water.

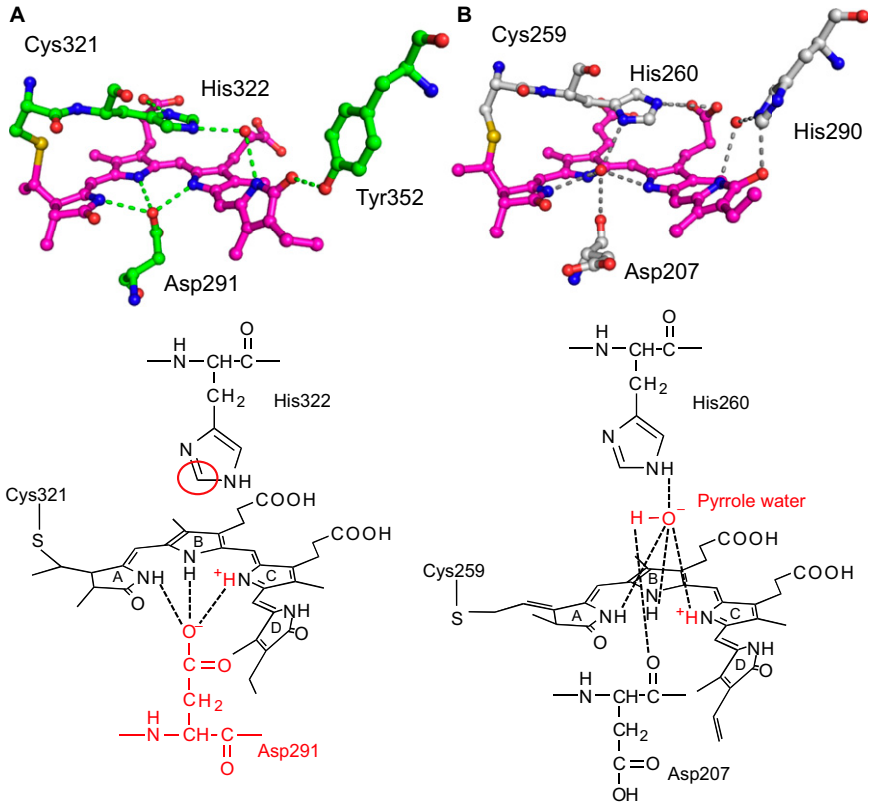

Fig. S6. Proposed protonation mechanism. Critical residues for chromophore binding (*Upper*) and possible protonation mechanism (*Lower*) in AnPixJg2 (*A*) and Cph1g (*B*) are shown. Asp291 is a potential proton donor in AnPixJg2, whereas the pyrrole water is a potential proton donor in Cph1g. Both potential proton donors are highlighted in red (*Lower*). Putative hydrogen bonds are shown as dotted lines.

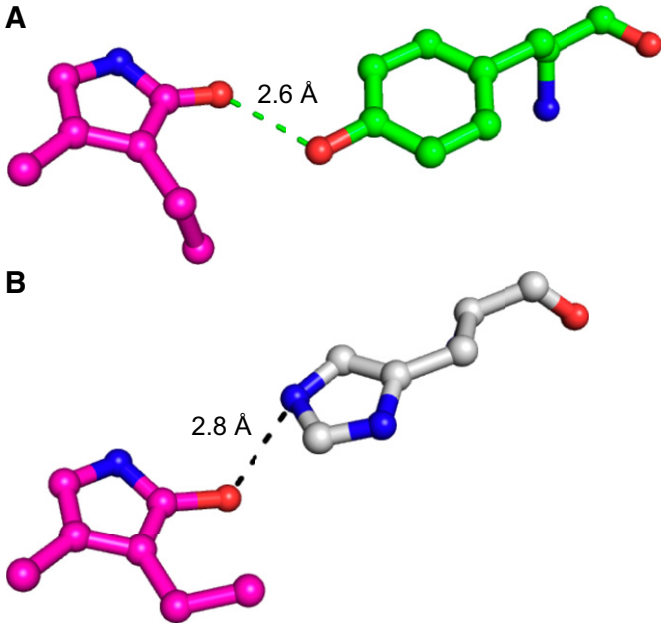

Fig. S7. Tyr352 (green) of AnPixJg2 (*A*) and His290 (gray) of Cph1g (*B*) that form hydrogen bonds with ring D carbonyl (pink).

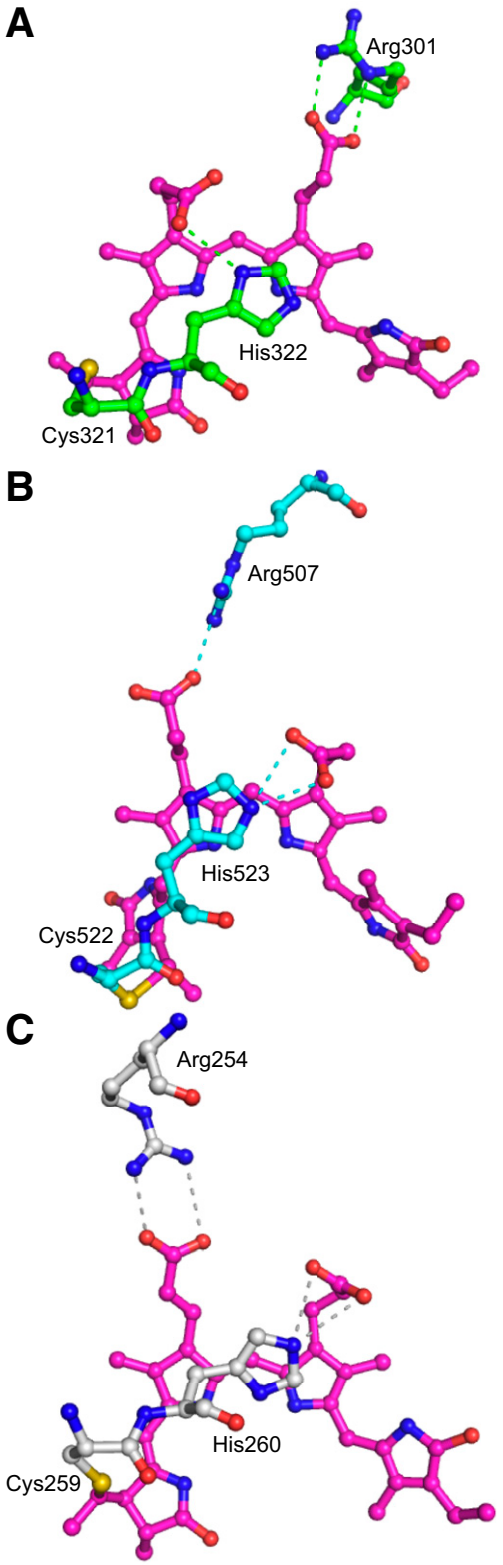

Fig. S8. Interaction of propionate chains and His/Arg residues of AnPixJg2 (*A*), TePixJg (*B*), and Cph1g (*C*).

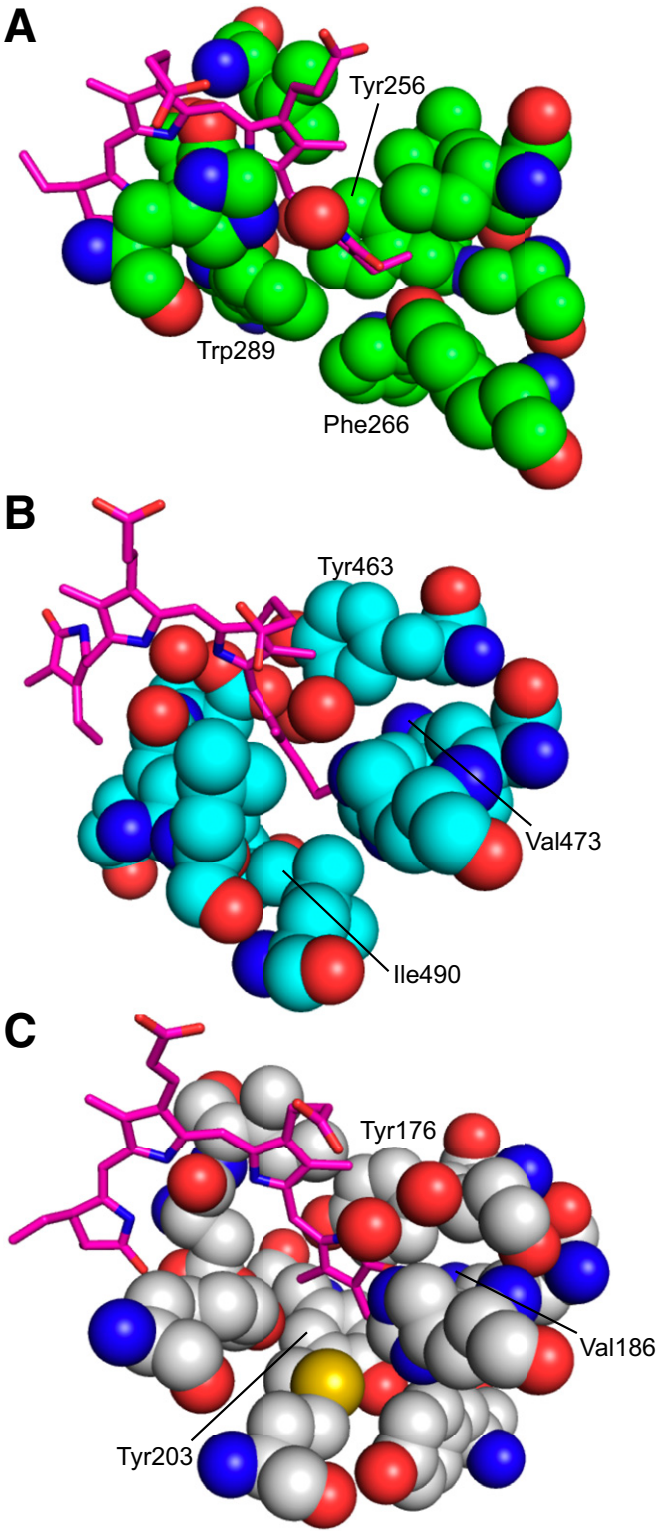

Fig. S9. Hydrophobic cavity of the ring D of AnPixJg2 (*A*), TePixJg (*B*), and Cph1g (*C*). It is obvious that the distance between Tyr256 on β1 strand and ring C nitrogen in AnPixJg2 (*A*) is farther than that between the corresponding Tyr176 and ring C nitrogen in Cph1g (*C*), as mentioned in the text.

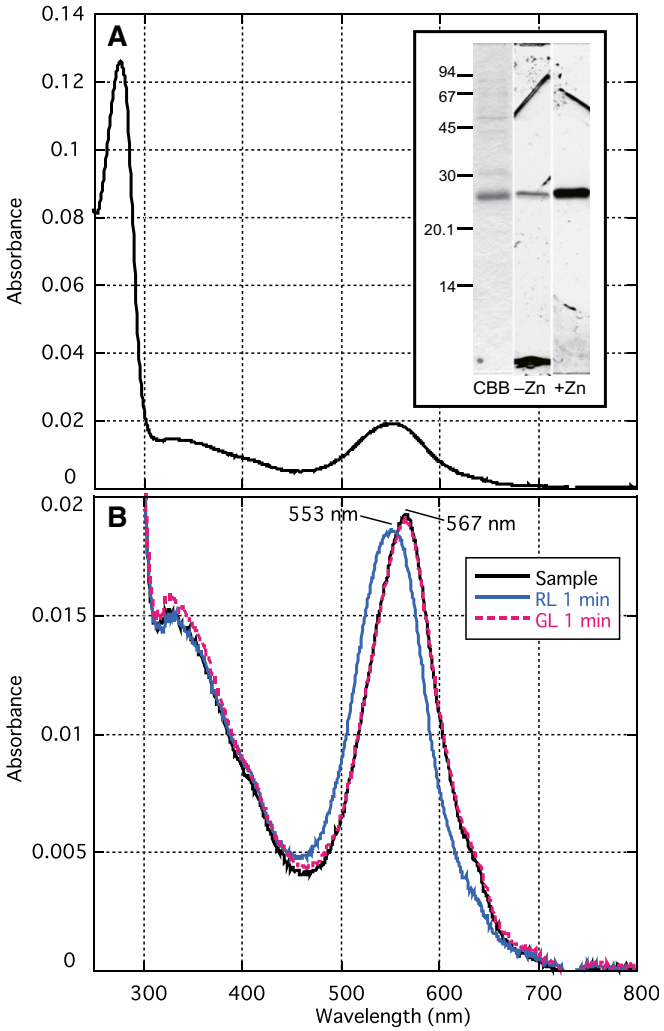

Fig. S10. Replacement of Trp289 with His residue. (*A*) Absorption spectrum of the sample after removal of imidazole. (*Inset*) CBB-staining and fluorescent SDS/PAGE of purified protein with or without 1 mM zinc acetate. (*B*) Absorption spectra of the sample after removal of imidazole (sample), its photoconverted form after irradiation with red light (RL) for 30 s and further photoconverted form after irradiation with green light (GL) for 30 s.

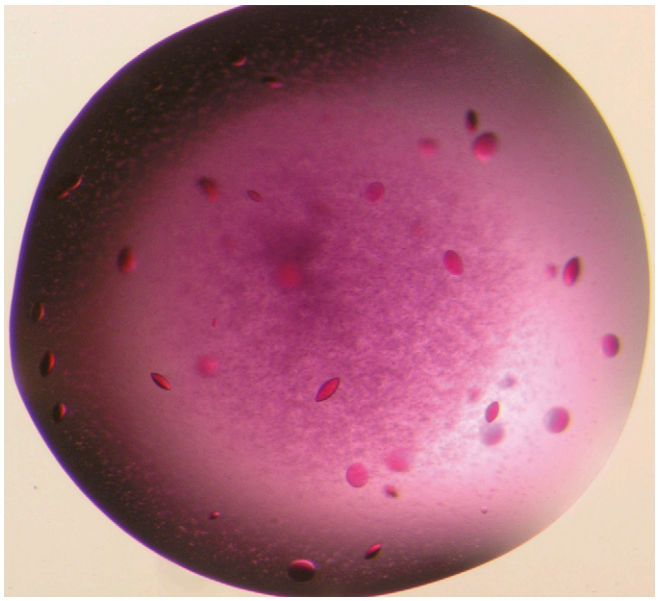

Fig. S11. Photography of the crystals of TePixJg Pg form.

Table S1. Data collection and refinement statistics of AnPixJg2 and TePixJg

Data set	AnPixJg2-Native	AnPixJg2-SAD	TePixJg-Native
X-ray source	PF-BL5A	PF-BL5A	PF-BL17A
Space group	$P4_32_12$	$P4_32_12$	$P6_5$
Unit-cell parameters			
a, Å	69.1		72.9
b, Å	69.1		72.9
c, Å	124.1		166.7
α, °	90		90
β, °	90		90
γ, °	90		90
Wavelength, Å	1.0000	1.6000	1.0000
Resolution range, Å	50.00–1.80 (1.86–1.80)*	50.00–2.20 (2.28–2.20)*	100.00–1.95 (2.02–1.95)*
Total reflections	389,475	792,364	292,703
Unique reflections	28,763	16,094	36,534
Completeness, %	99.7 (98.9)*	100 (99.9)*	92.9 (71.0)*
$R_{merge}(I)$, %†	5.7 (39.9)*	7.4 (49.7)*	5.8 (56.6)*
I/σ	15.9 (5.0)*	7.5 (3.5)*	26.0 (2.2)*
Phasing			
No. of sites		4	
Overall figure of merit			
Initial phasing		0.276	
After density modification		0.758	
Refinement			
Resolution, Å	28.31–1.80		59.02–2.00
R_{work}/R_{free}	19.7/22.4		18.7/22.3
No. atoms			
Protein	1471		2476
Ligand/ion	44		106
Water	185		111
Mean B factors, Å†	29.467		34.084
rmsd			
Bond length, Å	0.015		0.020
Bond angles, °	1.519		1.495

*Values in parentheses are for the highest resolution shells.

†$R_{merge}(I) = \Sigma|I(k) - \langle I\rangle|/\Sigma I(k)$, where $I(k)$ is the value of the kth measurement of the intensity of a reflection, $\langle I\rangle$ is the mean value of the intensity of that reflection, and the summation is overall measurement.